

Matteo Blandino¹, Marco Maria Molinari¹, Jacopo Liberatori¹, Pietro Paolo Ciottoli¹ & Riccardo Malpica Galassi¹

¹Sapienza Università di Roma, 00184, Rome, Italy

Abstract

We present a general framework for the design of sustainable hybrid aircraft which pursues minimal renewable energy consumption and climate effect. Thus, the approach takes into account the complete well-to-wake energy route, from the primary energy source to the aircraft end use, including the simultaneous usage of multiple energy carriers, such as electricity and sustainable aviation fuels (SAFs) obtained via different pathways. The framework builds on well-established hybrid aircraft design models, and accounts for unknown battery performances considering e_{bat} as a parameter. Nowadays and future leading-edge technologies such as Direct Air Capture (DAC) are investigated within a Life-Cycle Assessment (LCA) framework to estimate the SAF production efficiency and the emissions for the on-ground processes. We test the approach on the design of a hybrid SAF/electric regional aircraft that minimizes the total Well-to-Wake (WTW) energy and the average temperature response (ATR), in addition to the maximum take-off weight and fuel consumption, searching for the optimal power ratio in five different scenarios of European electric grid mix and Fischer-Tropsch SAF processing pathway. Results show that the impact of different Well-to-Tank (WTT) scenarios is more significant than adopting the optimal power management strategy. Nevertheless, by coupling these two aspects, an aircraft design with minimal climate impact and comparable to the baseline regional configuration can be achieved.

Keywords: Hybrid Propulsion, Life Cycle Assessment, Aircraft Optimization

1. Introduction

Air traffic has steadily increased since the last century, reflecting the expanding global connectivity and economic interdependence. However, the COVID-19 pandemic represented a major setback, disrupting air travel significantly. According to forecasts by the International Air Traffic Association (IATA), passenger numbers were expected to recover to 4 billion by 2023, reaching 103% of the 2019 figures, and were projected to ascend to 111% relative to 2019 by 2025 [1]. Aviation contributes to anthropogenic climate change through aircraft emissions (including carbon dioxide, nitrogen oxides, water vapor, soot, and sulfate aerosols), alongside increased cloudiness due to contrail formation. In particular, in 2018 - before the pandemic-related decline in flight numbers - the aviation industry accounted for 2.5-4% of global anthropogenic CO_2 emissions [2]. The European Commission has set the objective of achieving carbon neutrality by 2050 [3]. This initiative includes significant interim targets, such as reducing greenhouse gas (GHG) emissions by 55% compared to 1990 levels by 2030. These regulatory measures have led to significant changes in the aerospace sector, encouraging a transition towards the exploration of novel propulsion designs and the incorporation of alternative jet fuels into traditional engine setups. The most obvious solution to reduce the aviation climate impact is the employment of Electric Motors (EMs). Several studies have demonstrated the potential of electrified propulsive architectures [4, 5, 6]. Nevertheless, the adoption of electrified powertrains seems to be limited to the general aviation class, primarily because of the low specific energy of batteries, resulting in significant battery mass [7, 8]. On the other hand, the employment of alternative fuels, such as Sustainable Aviation Fuel (SAF) or liquid hydrogen, can further reduce the

climate impact, dramatically reducing the CO_2 emissions [9, 10]. However, the adoption of the latter solution comes with considerable risks due to the wide flammability limits and deflagration index of hydrogen [11]. Additionally, the onboard integration of hydrogen tanks would result in an increment of the aircraft Maximum Take-Off Weight (MTOW), consequently leading to higher energy consumption [12]. On the other hand, the previously mentioned solution—sustainable fuels—represents the most immediate way to meet stringent regulations. They require no major aircraft or engine redesign while ensuring lower, or even zero (depending on production methods), net CO_2 emissions. In alignment with this objective, the European Green Deal targets providing at least 2% SAF supply to EU airports in the near term, with a vision of achieving 70% by 2050 [13]. Currently, the utilization of alternative fuels is certified up to a 50% blending ratio with traditional kerosene [14], as their distinct physicochemical properties can impact the engine's in-flight performance [15].

Either way, a widely accepted view is that achieving carbon neutrality requires a combination of multiple engineering and regulatory solutions [16]. Consequently, all potential solutions should be explored. In the context of electrified propulsion, extending this technology to transport aircraft, particularly in categories A and B, can be accomplished through hybridization. The main idea is that the issues associated with electric propulsion can be mitigated by integrating the electric energy supply with a conventional powertrain [17]. Various power sources can be combined in different propulsion and aircraft architectures, leading to innovative design outcomes. Designing new aircraft concepts requires adapting or extending traditional methodologies [18, 19] to incorporate multiple power sources [5, 20, 21]. Significant improvements in batteries and electric motors are expected by 2050 [22], and many studies have examined the impact of technological uncertainties on optimized aircraft design [23, 24].

Considering the majority of studies present in the literature, when combining energy sources, like fuel and batteries, a multidisciplinary optimization of new design variables to achieve minimal maximum takeoff weight (MTOW) and fuel consumption [25, 26] have been performed. The works mentioned above focus on the aircraft system: this Tank-to-Wake (TTW) approach does not take into consideration the emissions and the energy consumption along the entire Life-Cycle (LC), from the energy source to the aircraft propulsion system, i.e., a Well-to-Wake (WTW) approach. In fact, a TTW method may lead to an optimized design that does not minimize the overall aircraft's Greenhouse Gas (GHG) contribution, particularly when using a SAF-driven thermal engine. Indeed, the efficiency and GHG contribution of SAFs depend greatly on the feedstocks and processing pathways used [27].

In this work, we introduce a novel framework for the preliminary design of aircraft that encompasses the efficiency and emissions of the energy carriers along the entire route from the primary energy source to the flying aircraft. Considering a renewable energy source, such as a wind turbine, the energy path splits into two branches: one supplies the SAF production, and the second charges the battery by going through the electric grid. Adopting a WTW approach, we optimize the on-board hybrid power management over five different scenarios that best represent the currently available and the long-term projected technologies. In addition to the classical objective functions, i.e., the maximum take-off weight and the fuel consumption, two new observables are included for the optimizer selection criteria: the total source energy required for one single mission and its related climate impact, described through the introduction of the ATR metric. With this approach, leading-edge techniques such as the Direct Air Capture (DAC) for the SAF production via the Fischer-Tropsch (FT) process can be included, paving the way towards aircraft concepts with negative emission technologies [28]. We demonstrate the validity of the employed preliminary design process by analyzing the results for a baseline regional aircraft. Subsequently, simple parametric study results are presented to assess the impactful effect of the WTW scenarios adopted in this work. Finally, the results of the optimization process are presented, demonstrating the leverages of the partial electrification of aeronautical engines.

The paper is organized as follows. The numerical methodologies for the aircraft preliminary sizing, the energy chain, and the climate model are explained in Section 2. Section 3 briefly describes the objective functions and design variables, together with the optimization workflow adopted in this paper. In Section 4, the baseline performance and mission specifications are presented, along with the different WTW scenarios. The results of the parametric and optimization analyses are discussed

in Section 5. Conclusions are summarized in Section 6.

2. Aircraft preliminary design

2.1 Aircraft model

In this section, we introduce the mathematical models that form the basis of the preliminary design framework utilized in this study. *PhlyGreen* is an object-oriented multi-disciplinary Python code that, reading the Top-Level Aircraft Requirement (TLAR) and mission specifications as inputs, conducts a preliminary sizing of the entire aircraft. The subsequent analysis focuses on a conventional two-propeller aircraft, hence disregarding the aero-propulsive effects of Distributed Propulsion (DP) [29, 30]. The starting point is the energy balance equation computed along the aircraft's relative *x*-axis:

$$\frac{P_p}{W_{TO}} = g \frac{1}{W_{TO}/S} qV C_D + \beta P_s, \tag{1}$$

where g is the gravity acceleration, $q=1/2\rho V^2$ is the dynamic pressure, $\beta=W(t)/W_{TO}$ is the instantaneous to take-off weight ratio, C_D is the drag coefficient, and P_s the specific excess power. In Eq.(1), the parameters q, C_D, β, P_s depend on the instantaneous flight condition, i.e., velocity V, altitude h and attitude. Consequently, this equation can be tailored to each of the performance constraints indicated by the TLAR, denoting one curve for flight phase, as shown in Fig. 1a. These curves identify a feasible space (light blue area), where the design-point (red circle) must be located.

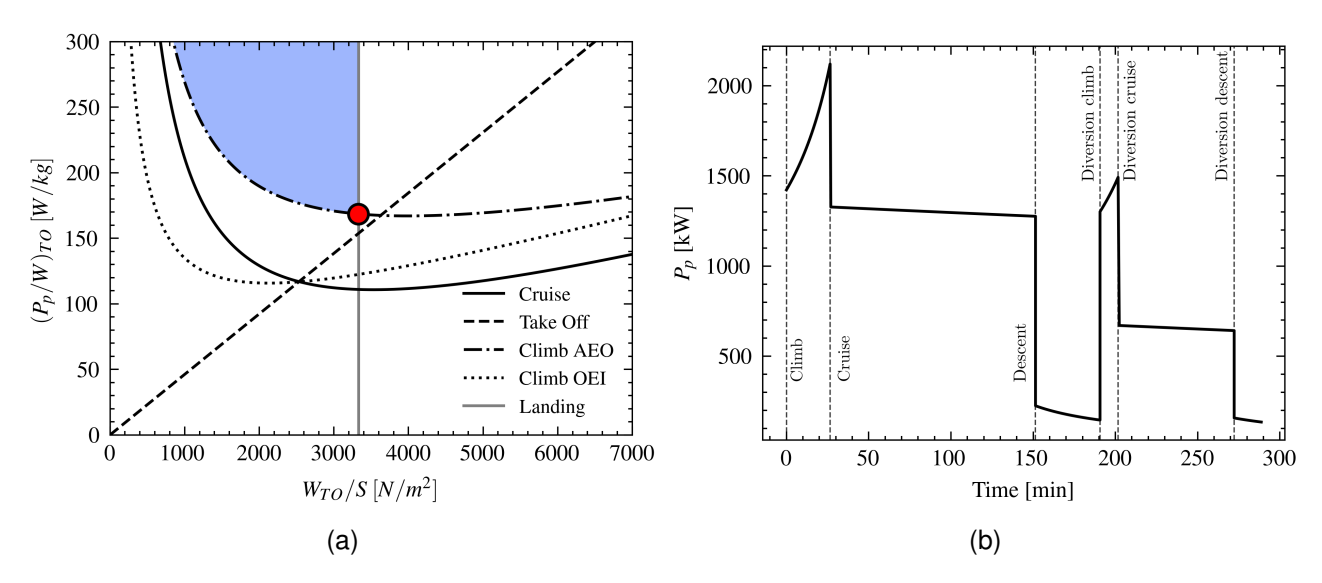


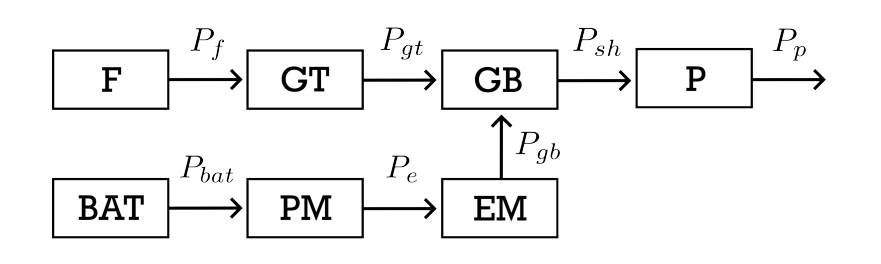
Figure 1 – (a) Power-loading diagram showing the design-point (red circle), (b) Propulsive power along the mission profile.

PhlyGreen is able to handle several hybrid-electric powertrain configurations, with multiple propulsive elements [30]. Considering the *hybrid-parallel* architecture shown in Fig. 2, the propulsive power P_p can be converted to the power outputs of each powertrain component. To achieve this for a hybrid propulsive system, we utilize the parameter introduced by Isikveren *et al.* [5], known as the *supplied power ratio*:

$$\varphi = \frac{P_{bat}}{P_{bat} + P_f} \in [0, 1] , \qquad (2)$$

representing the portion of electrical power used by the engine on the total power reserve. Since the considered aircraft presents only one kind of propulsive element, no more parameters are needed to describe the engine operating mode.

The graph depicted in Figure 2 illustrates the pathways from the power sources to the propulsive element. All the algebraic relations between the powertrain components can be recast to form a linear system of equations of the form $\sum P_{out} = \eta \sum P_{in}$, that can be specified for the investigated powertrain architecture:



Name	Component
F	Fuel
GT	Gas turbine
GB	Gearbox
BAT	Battery
PM	Power management
	and distribution system
EM	Electric motor
Р	Propulsive element

Figure 2 – Schematic model of a *parallel-hybrid* powertrain architecture.

Table 1 – Acronym of powertrain components

The elements of the matrix on the left-hand side can be dependent on the flight conditions and engine operating conditions. Starting from the propulsive power profile (shown in Fig. 1b) and solving the system of Eq. 3, the values of the required fuel and battery powers can be determined. These values can subsequently be integrated along the mission profile to determine the cumulative energy contributions from the electric and thermal engines:

$$E_i = \int_{t_s}^{t_e} \frac{P_i}{W_{TO}} \left(\varphi(t), \beta(t), h(t), V(t), \frac{W_{TO}}{S} \right) W_{TO} dt, \qquad (4)$$

where the index i is representative of the fuel and battery sources. To quantify the total energy ratio spent over a mission, it is necessary to introduce the integral energy split Ψ :

$$\Psi = \frac{E_{electric}}{E_{fuel} + E_{electric}} \,. \tag{5}$$

The energetic outcomes of the mission analysis can be converted into fuel weight W_{fuel} and battery weight W_{bat} , respectively, using their corresponding energy and power densities. The total weight breakdown is completed by the Operative Empty Weight (OEW) W_{OE} and payload W_{PL} :

$$W_{TO} = W_{fuel} + W_{bat} + W_{PL} + W_{OE}$$
 , (6)

$$W_{OE} = W_{ST} + W_{PT} + W_{crew} (7)$$

In Eq. 6 and 7, the values for the payload W_{PL} and the onboard personnel W_{crew} weights are determined by the TLARs. The structural weight W_{ST} is calculated using the Class I statistical formulation [31] for regional aircraft, while the powertrain weight is estimated as the ratio of the maximum shaft power that the engine must deliver during the mission to the specific power of the components of the chosen architecture [30], including EM and Power Management and Distribution System (PMAD). Given that a value of take-off mass is needed in Eq. 4 during the mission integration, the weight estimation necessitates an iterative procedure to converge to a final W_{TO} value. Fig. 5 shows a visual representation of the described procedure.

2.2 Energy chain

This study explores various pathways for generating synthetic aviation fuel and for the production and storage of electric power, to evaluate the potential benefits of integrating CO_2 -to-SAF fuels within a hybrid electric aircraft. The production of e-fuel is modeled through four key stages. The primary step

is the capture of carbon dioxide as a carbon feedstock from the concentrated carbon emissions of an ethanol refinery [32]. Secondarily hydrogen production is considered through electrolysis or Steam Methane Reforming (SMR). For electrolysis, two technological processes are examined. The first type, Proton Exchange Membrane (PEM) electrolysis, is known for its efficiency and adaptability to renewable energy sources, producing gaseous hydrogen. The second type, Solid Oxide Electrolysis Cells (SOEC), operates at high temperatures, typically above 1000 K, and is combined with electricity generation from High-Temperature Gas-Cooled Reactors (HTGR), providing a highly efficient and low-carbon energy source. SMR, although traditionally associated with fossil fuels, is evaluated as a transitional technology with the potential for integration with Carbon Capture and Utilization (CCU) to mitigate emissions. Following hydrogen production, the Reverse Water-Gas Shift (RWGS) reaction is employed to convert CO_2 and hydrogen into syngas, a mixture of carbon monoxide and hydrogen, which serves as a precursor for liquid fuel synthesis. Finally, the FT process converts syngas into liquid hydrocarbons, including synthetic kerosene suitable for aviation. This step is critical for producing high-quality, drop-in fuels that meet stringent aviation standards. Additionally, this paper examines the implications of different electricity sources for the overall life-cycle emissions and sustainability of the production processes. Three scenarios are analyzed: the current European grid mix of 2021 [33], which reflects a combination of fossil fuels, nuclear, and renewable energy sources; the projected European grid mix for 2050 [34], anticipating significant decarbonization efforts with a greater reliance on renewable energy and reduced fossil fuel usage; and a scenario exploring the use of entirely renewable electricity from sources such as wind turbines, aiming for a zero-emission supply chain [35].

The Well-to-Tank (WTT) analysis in Life Cycle Assessment (LCA) represents a valid instrument to evaluate the energy yield and the CO_2 emissions due to the entire chain preceding combustion or operational use of the energy carrier under consideration. This approach facilitates a comprehensive comparison of various supply production pathways and their adherence to regulatory standards, such as the Renewable Energy Directive 2018/2001 (RED II) [36] and the U.S. Renewable Fuels Standard (RFS) [37]. To conduct this study, the aviation industry has developed tools such as the Carbon Offsetting and Reduction Scheme for International Aviation (CORSIA) [38] and the Greenhouse gases Regulated Emissions and Energy use in Technologies Model (GREET) [35].

The energy chain definition begins with the characterization of the input resources properties, including density, lower heating value, carbon ratio, market value, allocation of energy, and emissions associated with the upstream process:

$$E(f) = a(f)E_{up}(f), (8)$$

$$EM(f) = a(f)EM_{up}(f) + a(f)\sum_{t \in T} s(f,t)EM_f(f,t).$$
 (9)

Here, E(f) and EM(f) represent the energy and emissions associated with the input resource f, respectively. Further, a(f) denotes the resource amount, $EM_f(f,t)$ is the emission factor linked to the generic technology t used upstream of the resource f, and s(f,t) is the share of various technologies. A primary resource, originating in nature, is associated with zero energy and emission burdens. It is noteworthy that within the LCA of SAF production, a resource derived from production waste unrelated to aviation fuel production is considered a primary resource [27].

Once the input resources are defined and characterized, the energy chain progresses through different stages, i.e., processes, are divided into stationary and transport processes and both are converted into a canonical model based on the mathematical input/output representation. The energy (per unit output) of the resultant resource f_o associated with the generic process is calculated as:

$$E_b = \frac{E(I) - E(P)}{a(f_o)(1 - l_r(f_o))},$$
(10)

$$E(I) = \sum_{f \in I} E(f). \tag{11}$$

Here, E(I) is the sum of various inputs in terms of energy, E(P) is the energy associated with coproducts, and $l_r(f_o)$ is the loss factor. Correspondingly, the output emissions can be calculated as:

$$EM_b = \frac{EM(I) - EM(P)}{a(f_o)(1 - l_r(f_o))}.$$
 (12)

Finally, the energy efficiency of the single process is determined by:

$$\eta_E = \frac{a(f_o)(1 - l_r(f_o))E_b}{E(I)}.$$
(13)

The overall WTT energy efficiency can be determined by building the entire process chain that a primary resource, like SAF or electricity, goes through. Fig.3 shows the complete WTW pathway of energy, from the production of electrical power from renewable sources to the end use on the hybrid aircraft, via either the electric grid or the SAF production.

Well-To-Tank (WTT) Tank-To-Wake (TTW) Renewable Energy Source η_{SAF} η_{EG} η_{EG}

Figure 3 – WTW pathways of renewable energy through electric grid and sustainable fuel production, the latter comprising electrolysis, carbon-capture or feed-stocks, FT synthesis, and transportation.

2.3 Climate Model

To evaluate and optimize the climatic impact of an aircraft, the primary challenge is to establish the most appropriate climate metric, defined as the system to quantify the climatic effects. Key climate metrics are outlined in [39], including Radiative Forcing, Global Warming Potential, Global Temperature Potential, and Average Temperature Response. Megill *et al.* [40] assert that, compared to the commonly used Global Warming Potential (GWP), the more accurate and suitable metrics for aerospace design and aviation policy-making are the Average Temperature Response (ATR) and the Effective Global Warming Potential (EGWP). The main advantages of these metrics include their stability and versatility over different time horizons, and emission scenarios, and neutrality towards different emitted species, due to the effective assessment of CO_2 -equivalents.

The method employed in this paper takes into account CO_2 , H_2O , NO_x , SO_4 , soot emissions, and the formation of persistent linear contrails. It relies on the standard atmosphere model and does not take into account local weather variations. However, in this work, it was not necessary to model the climatic impact of contrails 1 . The method is based on the calculation of the ATR [43, 44], which is the average, calculated over a certain time horizon, of the change in the mean surface temperature of the Earth $\Delta T(t)$ due to emissions from the aircraft, evaluated at a design point, a mission, and an emission scenario:

$$ATR_H = \frac{1}{H} \int_0^H \Delta T(t) dt \quad . \tag{14}$$

¹According to the method developed by Schumann [41], one of the necessary conditions for the formation of persistent condensation trails is that the atmospheric temperature is below -38 °C, which, conforming to the standard atmosphere model, is the case at altitudes above about 8150 m. In this work, which deals with turboprop aircraft, the altitudes considered are well below this threshold, therefore the climate impact model - as developed in [42] - would not detect the effect of contrails.

This metric strikes a balance between the computational resources required for preliminary design analysis and the precision and clarity of the outcomes. As discussed by Proesmans et~al.~ [42], a time horizon of H=100 years permits to assess a balanced result considering both the short-lived species as the ozone O_{3s} and the enduring atmospheric forcing effects. The change of surface temperature $\Delta T(t)$ is calculated using the annual emission of the relevant species, coupled with a fleet scenario that models the number of operational flights. $\Delta T(t)$ is calculated, according to the linear model of Sausen e Schumann [45], as the integral of convolution between the forcer $RF^*(\tau)$ (assumed zero for $t < t_0$) and the impulse response function $G_T(t)$ as defined in [46]:

$$\Delta T(t) = \int_{t_0}^t G_T(t-\tau)RF^*(\tau)d\tau \quad . \tag{15}$$

The impulsive response function is the system's response when the forcing is a Dirac delta. Its expression, obtained by approximating the results of a General Circulation Model (GCM) atmosphere-ocean simulation [47, 48], results in:

$$G_T(t) = \alpha e^{-t/\tau}$$
 where $\alpha = \frac{2.246}{36.8} \frac{K}{yr}$ and $\tau = 36.8 \, yr$. (16)

The radiative forcing RF is a measure of the alteration of the balance between incoming and outgoing energy in the Earth-atmosphere system due to a certain factor, for example an increase in the atmospheric concentration of a chemical species. A positive value of RF indicates an overheating of the Earth's surface. $RF^*(\tau)$ is the sum of the radiative forcings associated with the different chemical species considered, each multiplied by its relative effectiveness, normalized with the radiative forcing corresponding to a CO_2 concentration in the atmosphere equal to twice the pre-industrial value [49]:

$$RF^{*}(\tau) = \sum_{i} \left(E_{i} \frac{RF_{i}(\tau)}{RF_{2xCO_{2}}} \right) , \qquad (17)$$

$$i = CO_{2}, CH_{4}, O_{3_{L}}, O_{3_{S}}, H_{2}O, SO_{4}, soot \qquad RF_{2\times CO_{2}} = 3.7 \frac{W}{m^{2}} \qquad E_{i} = \frac{\lambda_{i}}{\lambda_{CO_{2}}} .$$

In Eq. 17 the i index represents the i-th species that contributes to the surface temperature change, while E_i are the efficacy parameters for each species [50]. Efficacies are calculated as climate sensitivities λ_i normalized with the value associated with carbon dioxide. Tab.2 shows the values assumed by the climate sensitivities λ_i and efficacies EFF $_i$.

CO_2			H_2O			
$\lambda_i \left[\frac{K}{W/m^2}\right]$	0.73	0.86	1.00	0.83	0.66	0.51
E_i	1.00	1.18	1.37	1.14	0.90	0.70

Table 2 – Climate sensitivities and efficacies of the species under consideration.

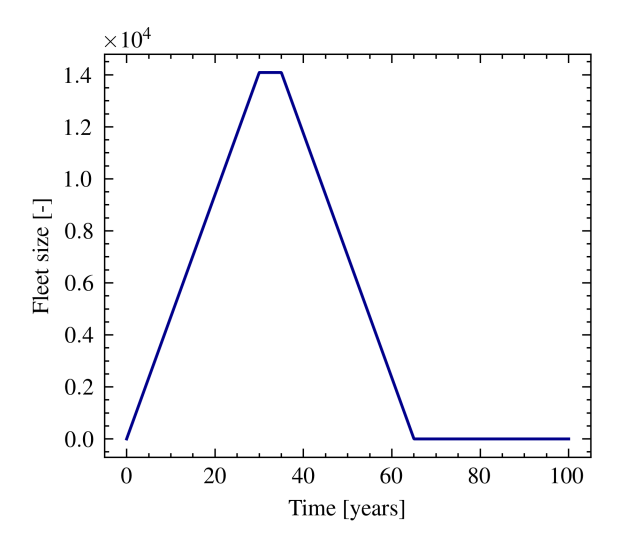
The radiative factors RF_i are calculated starting from the emissions along a single mission, considering both the *in-flight* and the *on-ground* operations. The former are assessed by considering pollutant emissions per mission, determined using the Emission Indices (EIs) listed in Table 3. The method proposed by Filippone *et al.* [51] is employed for calculating NO_x emissions, which are dependent upon engine operating conditions. Regarding the other contribution, the *on-ground* emissions are calculated using the WTT methods described in Sec 2.2, applied to both fuel and electricity production.

	CO_2	H_2O	SO_4	Soot
$EI_i [g/kg]$	$3.16 \cdot 10^3$	$1.26 \cdot 10^3$	0.2	$0.4 \cdot 10^{-1}$

Table 3 – Emission Indices independent of engine operating conditions [52].

The ATR_{100} estimation requires a hypothetical fleet scenario. Considering the actual ATR-42 fleet, as of May 2024, there are 211 documented active aircraft [53]. Nevertheless, to ensure a fair comparison

with previous works [42, 54], a similar scenario is adopted. Starting from the year 2020, when the designed aircraft would be introduced into the market, and assuming an aircraft operating lifetime of 35 years, the peak productivity would be reached in the period between the years 2050 and 2055. Considering an operative period of 65 years, the fleet would be dismissed by the year 2085. The resulting scenario over the selected time horizon is shown in Fig. 4.



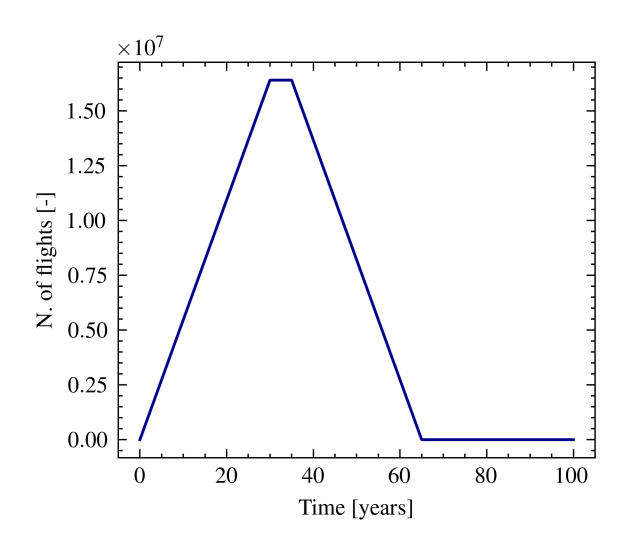


Figure 4 – Fleet size and number of operated flights for the hypothetical scenario.

3. Methodology

3.1 Optimization framework

The present work is based on a Multidisciplinary Design Optimization (MDO) problem, with the inner core represented by the PhlyGreen code presented in Sec. 2.1. Figure 5 shows a graphic representation of the optimization loop, with a highlight on the aircraft preliminary sizing procedure. In the following, four different objective functions will be considered: the maximum take-off weight W_{TO} , the fuel consumption W_F , the total source energy, and the ATR_{100} . The first two objectives are commonly used target variables in most optimization problems [55, 25], while the latter two, to the authors' knowledge, have not been previously utilized. As discussed in section 2.2, the SAF production chain comprises several sources of GHG emissions, such as the fuel transportation stage, and significant energy inefficiencies. Therefore, the electric energy branch may be favored even at the cost of a heavier aircraft. Due to the conflicting nature of the objective functions, a Genetic Algorithm (GA) can be employed as the optimizer driver algorithm to converge toward a set of optimal solutions quickly, avoiding getting stuck into suboptimal solutions. Given the high number of objective functions, to prevent the clustering of solutions along a single Pareto front and to promote diversity among the solutions, the Non-dominated Sorting Genetic Algorithm (NSGA-II) is chosen. An initial population of 1000 individuals is generated by Latin Hypercube Sampling (LHS) with a random seed and each generation is composed of 200 offspring populations. The entire process has been implemented using the python library pymoo [56]. The optimization process stops when no dominant solution is discovered after 3 generations. No constraints will be imposed on the optimizer to ensure a comprehensive exploration of the design space. Considerations regarding the certification specifications of the selected aircraft class will be addressed later in the results section.

3.2 Design variables

The design methodology is focused on the on-board energy management. The supplied power ratio φ , as outlined in Eq. 4, is an instantaneous value that can be adjusted to attain the optimal configuration concerning the defined objectives. To reduce the number of design variables, φ is modeled with a linear trend within each mission segment, hence it is fully defined by the initial and final values. To explore a wider solution space, the initial supplied power ratio of the i-th phase is not forced to be

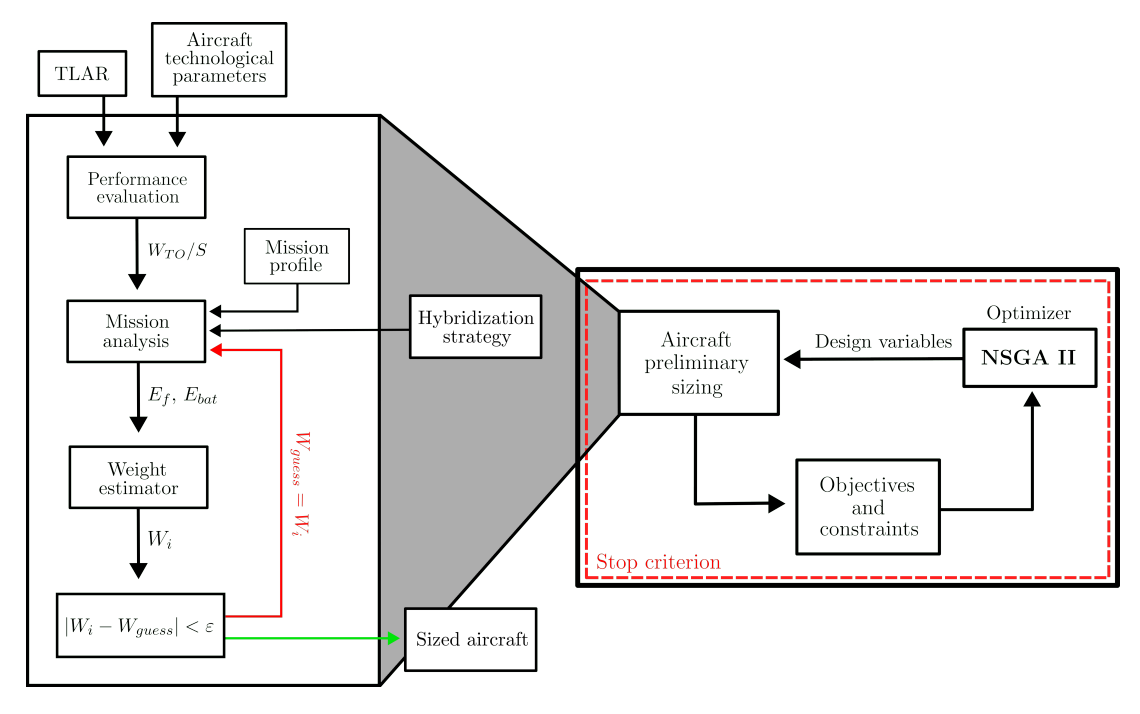


Figure 5 – Workflow representation of the MDO problem.

equal to the final value of the (i-1)-th phase, leading to a discontinuous piece-wise function. Therefore, the optimizer will search for the optimum by considering the initial and final φ values as Design Variables (DVs). In this study, five supplied power ratios, as listed in Table 4, will be used to identify the optimal solutions among the objective functions described in the previous subsection.

Design variable	Range	Units
Supplied power ratio at take-off, $\varphi_{take-off}$	[0.0, 1.0]	-
Initial climb supplied power ratio, $\varphi_{climb,s}$	[0.0, 1.0]	-
Final climb supplied power ratio, $\varphi_{climb,e}$	[0.0, 1.0]	-
Initial cruise supplied power ratio, $\varphi_{cruise,s}$	[0.0, 1.0]	-
Final cruise supplied power ratio, $\phi_{cruise,e}$	[0.0, 1.0]	-

Table 4 – Design variables for the optimization problem.

4. Test case description

For the following analysis, a baseline aircraft configuration needs to be established. The mission and performance specifications will be detailed in Section 4.1, which will also include a validation based on the ATR-42 configuration. Section 4.2 will describe the five scenarios concerning the fuel-electricity source combinations.

4.1 Top-Level Aircraft Requirements (TLARs)

For this study, a regional aircraft with a capacity of 48 passengers is selected. The model is based on the ATR 42-600, a twin-engine aircraft designed for short to medium-range missions. The ATR 42, along with its larger counterpart, the ATR 72, has been extensively utilized in the analysis of hybrid-electric powertrains [57, 30].

The TLARs are detailed in Tab. 5. The mission consists of a design range of 750 NM with a maximum payload of 4650 kg. The cruise is conducted at constant Mach number $M_{cr}=0.45$ at a cruise altitude of 8000 m. The aircraft must be capable of achieving in One Engine Inoperative (OEI) conditions a balked landing at 1.2 times the approach velocity, set at V=53.5 m/s, with a climb gradient of 0.021%. Additionally, the maximum take-off field length $s_{TO}=950$ m imposes a constraint on the take-off. Moreover, in the event of an alternate landing, a diversion phase with a range of 200 NM, conducted

at $M_{div}=0.2$ and an altitude of 3100 m, must be considered. The take-off and landing phases will be neglected in the following mission integration. Nonetheless, the fuel consumed during these phases will be accounted for using Roskam's fuel fractions [18]. These performance constraints result in the selection of a wing loading of 3328 N/m^2 . Finally, as concerns the climb and descent phases, the velocity is regulated to achieve the minimum drag condition. The aircraft design and technological parameters that will be considered as fixed are listed in Tab. 6. The maximum lift coefficient and wing aspect ratio are based on the ATR 42 geometry and are deliberately maintained constant to explore the potential of integrating new technologies into existing architectures.

Range 750 NM Payload 4650 kg Cruise Mach number 0.45 - Cruise altitude 8000 m Approach velocity 53.5 m/s OEI climb gradient 0.021 -
Cruise Mach number 0.45 - Cruise altitude 8000 m Approach velocity 53.5 m/s OEI climb gradient 0.021 -
Cruise altitude 8000 m Approach velocity 53.5 m/s OEI climb gradient 0.021 -
Approach velocity 53.5 m/s OEI climb gradient 0.021 -
OEI climb gradient 0.021 -
•
Take off field length OFO m
Take-off field length 950 m
Diversion range 220 NM
Diversion Mach number 0.2 -
Diversion altitude 3100 m

Parameter	Value	Units
Maximum lift coefficient, $C_{L,max}$	1.9	-
Wing aspect ratio, AR	11	-
Fuel lower heating value	43.5	MJ/kg
Gas turbine efficiency, η_{GT}	0.22	-
Propulsive efficiency, η_P	0.75	-
Gearbox efficiency, η_{GB}	0.96	-
PMAD efficiency, η_{PM}	0.99	-
Thermal engine specific power	3.6	kW/kg
Electric motor specific power	7.7	kW/kg
PMAD specific power	2.2	kW/kg

Table 5 – TLAR.

Table 6 – Fixed parameters.

Before delving into the analysis involving hybrid powertrain architectures, it is useful to discuss the validity of the multi-disciplinary framework introduced in Sec. 2.1. Considering the ATR 42-600 datasheet [58], the preliminary design is performed over the maximum-range mission reported in Tab. 5.

Parameter	Value	Reference	Difference
Take-off weight, W_{TO} [kg]	18846.43	18600	1.3%
Operational Empty Weight, OEI [kg]	11811.31	11750	0.5%
Powertrain weight, W_{PT} [kg]	1016.02	960	5.8%
Wing surface, $S[m^2]$	55.54	54.5	1.9%
Block fuel (400 NM range), $W_{F,400}$ [kg]	1059.23	1019	3.9%
Block fuel (design range), W_F [kg]	2583.60	-	-
Average temperature response, ATR_{100} [mK]	3.87	-	-
Source energy [GJ]	119.92	-	-

Table 7 – Comparison between the preliminary design outcome with the reference ATR 42-600 data.

Table 7 shows a strong agreement between the preliminary design results and the reference values, with the maximum difference being 5.8% observed in the powertrain weight. This variation can be attributed to the statistical model utilized for powertrain sizing. However, following the aircraft's design for the maximum-range mission, conducting a test on a shorter mission yields a block fuel value with a discrepancy of 3.9%, which is deemed acceptable for a preliminary design process. It is important to note that the exact mission profile is unknown to the authors, and the slight differences in the results may be attributed to this uncertainty. In addition, the remaining objective functions are reported in Tab. 7, to ensure a comparison with optimized designs in the following.

4.2 Well-To-Tank Scenarios

In Table 8, we present five scenarios of interest: four for Power-to-Liquid (PtL) fuel production and one for conventional fuel from crude oil with a 2021 distributed electricity mix (Jet A1 + EU 2021). The results from the GREET module are defined on an energy basis ($[MJ^{-1}]$), for both FT and con-

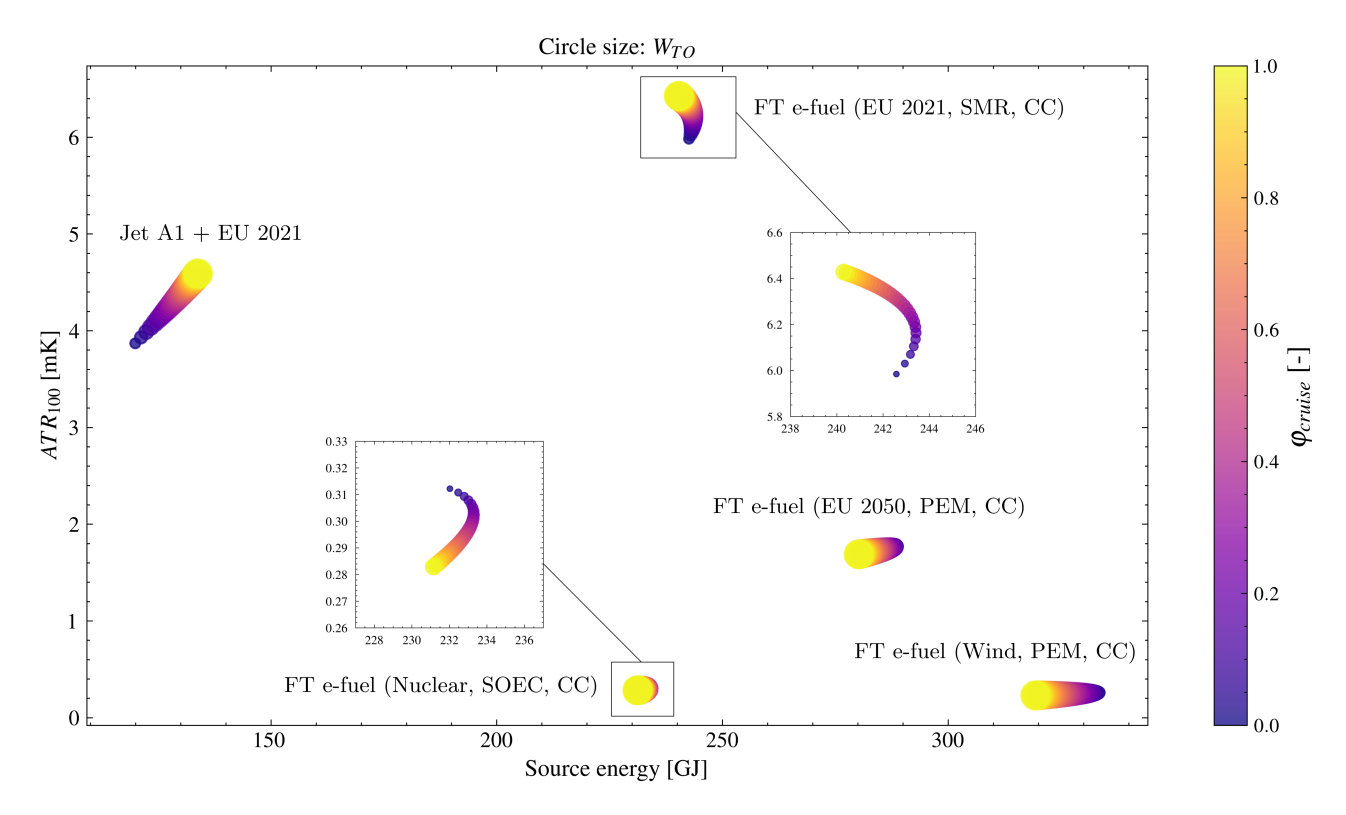


Figure 6 – Effects of the cruise supplied power ratio φ_{cruise} with $e_{bat}=1$ kWh/kg on the required source energy and the climate impact metric ATR_{100} . The circle size represents the take-off weight W_{TO} .

ventional fuels. The overall energy efficiency η_{WTT} of each process is determined by the ratio of the functional unit to the total energy input, which includes both the functional unit and any associated losses. For GHGs, the functional unit is expressed in terms of CO_2 equivalent emissions $(CO_{2_{eq}})$, which standardizes the impact of various greenhouse gases using carbon dioxide as a reference [59, 60]. The analysis, being solely focused on energy aspects and not on the large-scale quantitative availability of fuel, does not consider environmental impacts and energy resources required for the construction of new facilities, or land use changes. The results indicate that, from an energy perspective, conventional jet fuel is the most efficient as it only involves the extraction and refining of crude oil. In contrast, the generation of e-fuel involves multiple processes that require energy, such as the production of hydrogen through electrolysis. In fact, from an environmental standpoint, the generation of e-fuel with an energy mix that does not heavily utilize renewable energy has a heavier impact than conventional kerosene. For this reason, the use of PEM technology with the current European grid mix is excluded from aircraft optimization, whereas SMR process is retained as it is considered the most feasible in the medium-term.

Scenario	$CO_{2,wtw}$ [g CO_2 /MJ]	$CO_{2,grid}$ [g CO_2 /MJ]	η_{WTT}
Jet A1 + EU 2021	$8.20 \cdot 10^{-3}$	$9.36 \cdot 10^{-2}$	0.89
FT e-fuel (EU 2021, SMR, CC)	$5.31 \cdot 10^{-2}$	$9.36 \cdot 10^{-2}$	0.44
FT e-fuel (EU 2050, PEM, CC)	$-3.74 \cdot 10^{-2}$	$1.08 \cdot 10^{-2}$	0.37
FT e-fuel (Wind, PEM, CC)	$-6.72 \cdot 10^{-2}$	0.0	0.32
FT e-fuel (Nuclear, SOEC, CC)	$-6.75 \cdot 10^{-2}$	$5.34 \cdot 10^{-4}$	0.46

Table 8 – WTT scenarios considered in the optimization process.

5. Results and discussion

5.1 Parametric analysis on WTT scenarios

In this section, before exploring the optimization process results, the impact of the WTT scenarios on a single mission is evaluated via a parametric analysis.

Fixing the battery specific energy to $e_{bat} = 1 \text{ kWh/kg}$, for the sake of simplicity, we impose a constant φ_{cruise} to vary as a parameter. In this manner, it is possible to break down the contribution of the different fuel and electricity generation routes with the on-board energy management effects. Figure 6 shows the results in terms of the two new objectives introduced in this work, the source energy and the ATR₁₀₀, for the five WTT scenarios depicted in Sec. 4.2. Firstly, it's worth noticing that, even if the battery specific energy has been set to an optimistic value [22], as the φ_{cruise} is incremented, the aircraft take-off weight grows up due to the extreme weight of the resulting battery pack. Starting with the Jet A1-fueled aircraft, since the fossil fuel is subjected to a traditional refinement process which is significantly cheaper than the PtL synthesis of e-fuels, the energy consumed during a single aircraft mission is the lowest among the cases studied. As the battery weight increases, both the objective functions deteriorate: notwithstanding the fuel consumption is reduced, the WTT battery branch leads to an increase in CO_2 emissions. The most interesting result comes from the FT fuel produced with today's electric grid technology. Under the same no-battery conditions, the climate impact of an aircraft burning present-day e-fuels is higher. Even if carbon capture techniques are used, the quota of CO_2 emitted due to the electricity required for fuel synthesis exceeds the amount of CO_2 captured from the atmosphere. When the same aircraft is hybridized, a slight reduction in the source energy is attained. When considering the 2050 projection for the electric mix, in which a larger share of energy comes from renewable sources, the e-fuel production chain becomes cleaner and more efficient. Considering the points in Fig. 6, the highly-reduced on-ground emissions result in a halved average temperature response with respect to the traditional kerosene. Nevertheless, the required energy reaches 290 GJ per flight, almost three times the baseline case, highlighting the necessity for more efficient PtL processes besides the adoption of renewable energy sources. The last two cases involving zero-carbon energy sources, namely nuclear and wind power, present the lowest climate impact, regulated only by the flight phases which are not hybridized. The discrepancy between these two lies only in the hydrogen dissociation process, with the SOEC being more efficient than the PEM technology.

From Figure 6, the most insightful considerations can be recovered by the individual effects of the WTT scenarios and the in-flight power management. As seen, the impact of hybridization is limited

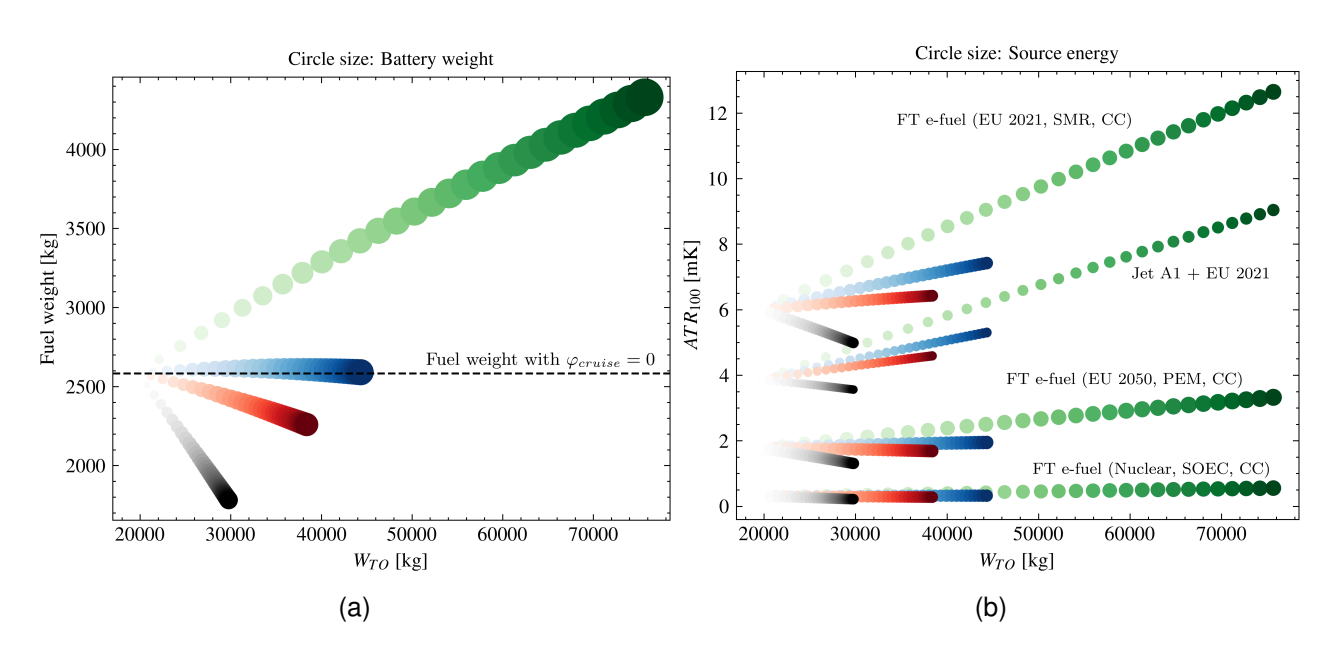


Figure 7 – Climate and aircraft performance, parametrized by φ_{cruise} (specified by color tonality). Battery specific energy are indicated by different colors: (•) $e_{bat} = 0.7$ kWh/kg, (•) $e_{bat} = 0.9$ kWh/kg, (•) $e_{bat} = 1.0$ kWh/kg, (•) $e_{bat} = 1.3$ kWh/kg.

compared to the energy consumption and emissions improvements expected by more efficient WTT routes.

The same parametric analysis has been carried out with different—both more pessimistic and more optimistic—battery specific energy e_{bat} . Considering the recent advancements in battery energy storage performance [61], four different battery specific energy are considered: $e_{bat}=0.7,\,0.9,\,1.0,\,1.3$ kWh/kg. Figure 7a shows how an increasing electric power supply changes fuel consumption. The lower heating value for the different kinds of fuels is kept constant, therefore, the fuel consumption will remain the same for each scenario. Looking at the results for the less-performing battery, the introduction of partial electrification triggers a snowball effect: instead of decreasing, the fuel required to complete the mission increases due to the rise in W_{TO} and the consequent need for greater propulsive power. The case at $e_{bat}=0.9$ kWh/kg represents a limit solution for the analyzed test case. As φ_{cruise} tends to unity, the fuel consumption is kept almost constant to the value with no electric power supply.

By increasing the battery's specific energy to 1.0 kWh/kg, a slight reduction in fuel weight is achieved, but this comes at the expense of designing a significantly heavier aircraft. Finally, the last case investigated in Fig. 7a, demonstrates that a fully electric cruise results in a reduction of 31% in fuel consumption with an increase in take-off weight of $\sim 50\%$. Fig. 7b reports the results of the above analysis in terms of ATR_{100} for the WTT scenarios. Referring to today's e-fuel case, the climate effect of a hybridized mission would be more significant than that of a traditional all-thermal aircraft, even if a high-performance battery is employed. The direction changes when the e-fuel is produced with the electric mix of 2050. As mentioned earlier, the average temperature response is approximately halved compared to the Jet A1 scenario. Improved battery performance results in a lighter battery pack, leading to a lighter aircraft, similar to the current configuration of regional airliners.

5.2 Optimization results

A multi-objective optimization process has been performed to obtain the optimal on-board power hybridization in each WTT scenario described in Sec. 4.2. In this process, the battery specific energy, considered as a deterministic parameter ranging from 0.6 kWh/kg to 1.5 kWh/kg, is fixed in each single optimization problem, and its impact on the Pareto fronts is analyzed. For brevity, the results of the fourth and fifth scenarios, involving nuclear and wind power, will be briefly discussed. Particular emphasis will be given to the WTT routes corresponding to the 2021 and 2050 European electric mix.

The results for the wind-powered electric grid scenario are shown in Fig. 8. To simplify the characterization of the hybridization effect, the integral energy split Ψ is used as a single parameter instead of the five DVs. Across the e_{bat} range, the main effect is the reduction of the maximum take-off weight

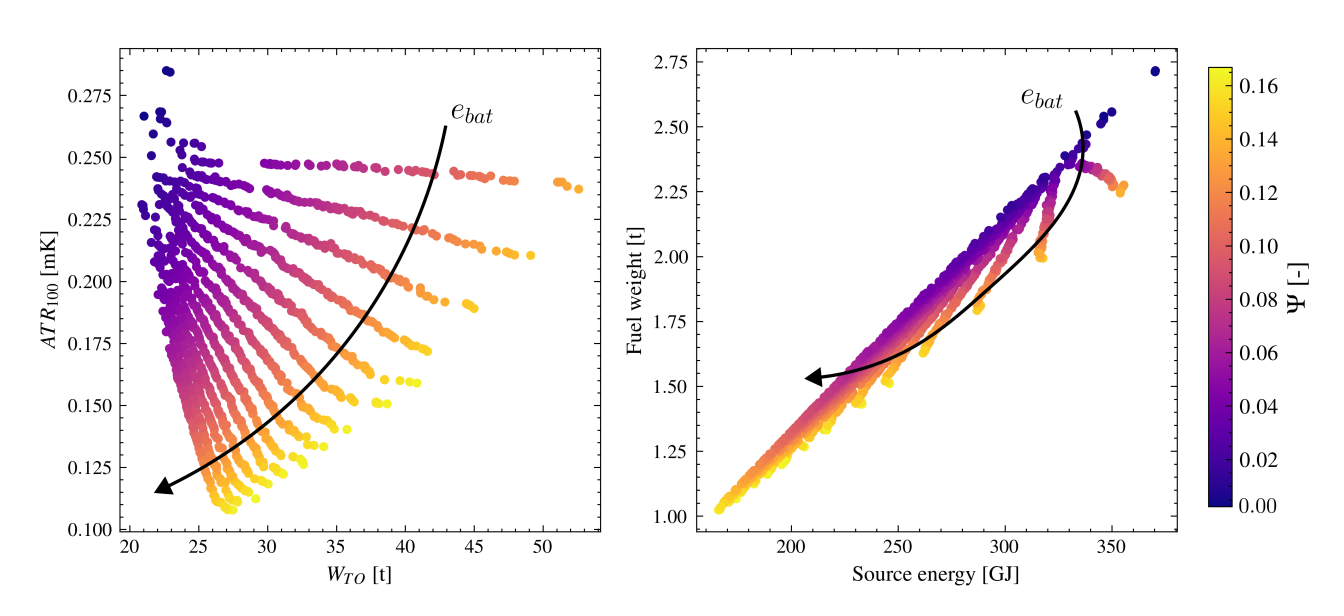


Figure 8 – Pareto frontiers for the FT e-fuel (Wind, PEM, CC) case.

due to the lighter battery. On the other hand, as Ψ grows along each front for $e_{bat} > 0.65$ kWh/kg, a reduction of source energy is obtained. However, in terms of climate impact, the temperature increase caused by an aircraft using wind-powered WTT is one order of magnitude smaller than that of a traditional aircraft. Therefore, an optimization based on the on-board power split is pointless with respect to an improvement in battery and e-fuel process technologies. The same observations remain valid for the nuclear-powered electric grid case.

Focusing on the currently available processes, Figures 9 and 11 present the Pareto-optimal solutions on parallel coordinate plots, obtained for the Jet A1 and FT e-fuel with the 2021 electric mix, respectively, with varying battery energy density e_{bat} . Firstly, the results show that the optimal value for the hybridization factor during the take-off phase never exceeds $\varphi_{take-off} = 0.4$, with a high-density distribution around the 20%.

This behavior is due to the limited specific power of the battery. The battery pack is sized according to the most demanding energy or power requirement along the mission and, increasing the supplied power during the take-off, the battery pack would be sized according to the take-off requirement. Another interesting optimal DV distribution is related to the hybridization strategy during the climb phase. In fact, less aggressive battery usage is preferred in the final stages of the climb, while the $\varphi_{climb,s}$ is uniformly distributed along the entire range and dependent on cruise electrification. Inspecting the results, the sixth column of Fig. 9 reports the ATR_{100} distribution. As expected, the main driving parameter which leads to the minimum climate impact is the battery specific energy. Hence, by adopting a power strategy tending to a fully electric configuration, a 30% improvement in the average temperature response can be achieved.

Nevertheless, to achieve a more comprehensive understanding of the results, the joint distributions of the DVs and objective functions are displayed in Fig. 10. The number of points in each Pareto front is fixed, thus the probability density functions reflect the distribution of the observables over the entire battery performance spectrum without any bias. The upper-left panel shows a quasi-linear correlation between the fuel consumption and the ATR_{100} . The predominant designs lie in the [3.0, 3.5] mK ATR_{100} and [1.5, 2.0] t W_F ranges. Considering the corresponding values in Tab. 7, an improvement of respectively the 22% and 41% can be attained by promoting electrified power management.

Figure 10b displays a clustered distribution in the maximum take-off weight W_{TO} , with the peak at 25000 kg, a value that exceeds the nominal ATR 42 W_{TO} by 33%. Fixing the wing loading, such a

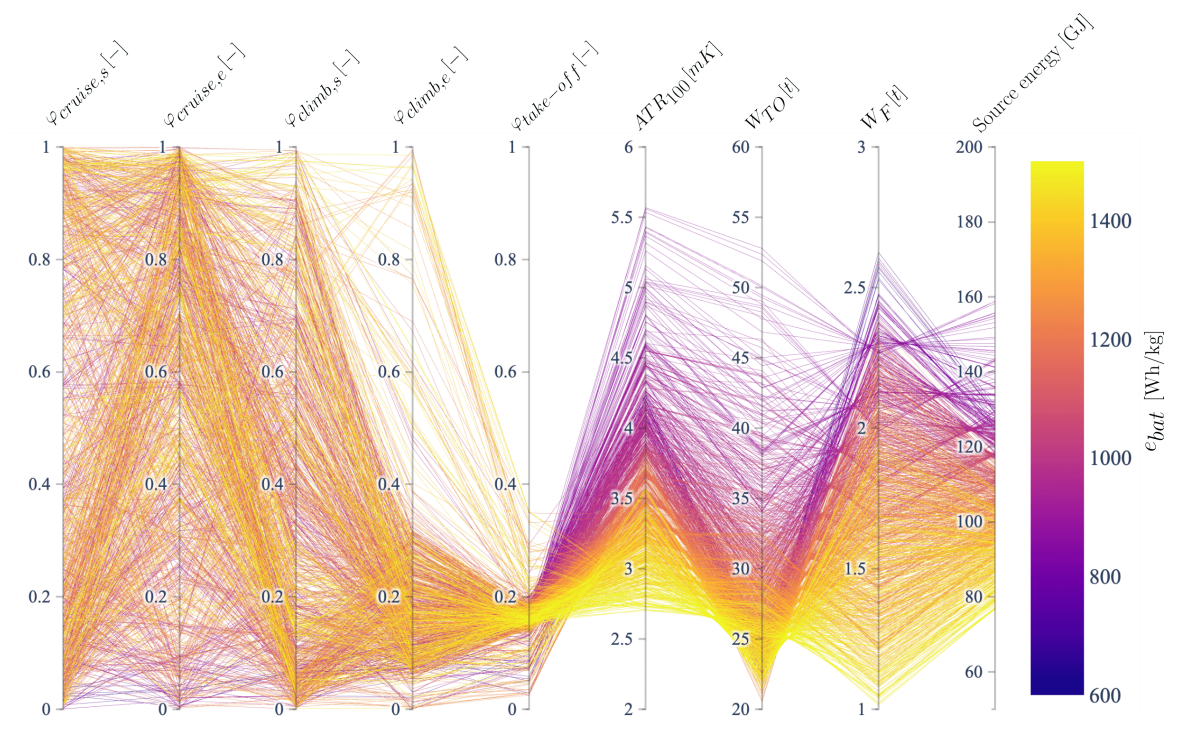


Figure 9 – Pareto-optimal solutions visualized on parallel coordinates (5 design variables and 4 objectives) for the Jet A1 + EU 2021 case.

weight increment results in a wing surface extension of $19m^2$, leading to an International Civil Aviation Organization (ICAO) C wingspan categorization [62].

The optimization results for the cruise hybridization levels are presented in Fig. 10c, where a strongly multi-modal distribution is observed. For cruise phases with low $\varphi_{cruise,s}$, the value of $\varphi_{cruise,e}$ is almost uncorrelated, displaying a practically uniform distribution. Conversely, a constant hybridization strategy is preferred when the cruise segment starts with full electrification. The last panel, showing the supplied power ratios during the climb phase, displays a considerably narrow marginal distribution around $\varphi_{climb,e} = 0.13$. Conversely, the starting climb supplied power ratio is more distributed into its range of variation, driven by the battery specific energy value. Returning to the propulsive power required along the mission (shown in Fig. 1b), the maximum occurs at the high-altitude segment of the climb phase. Therefore, the optimizer avoids the scenarios where the battery needs to deliver the peak power at top of climb.

Substituting the traditional Jet A1 with the e-fuel produced with currently available technologies, a different distribution of optimal designs is obtained, as displayed in the parallel coordinates plot of

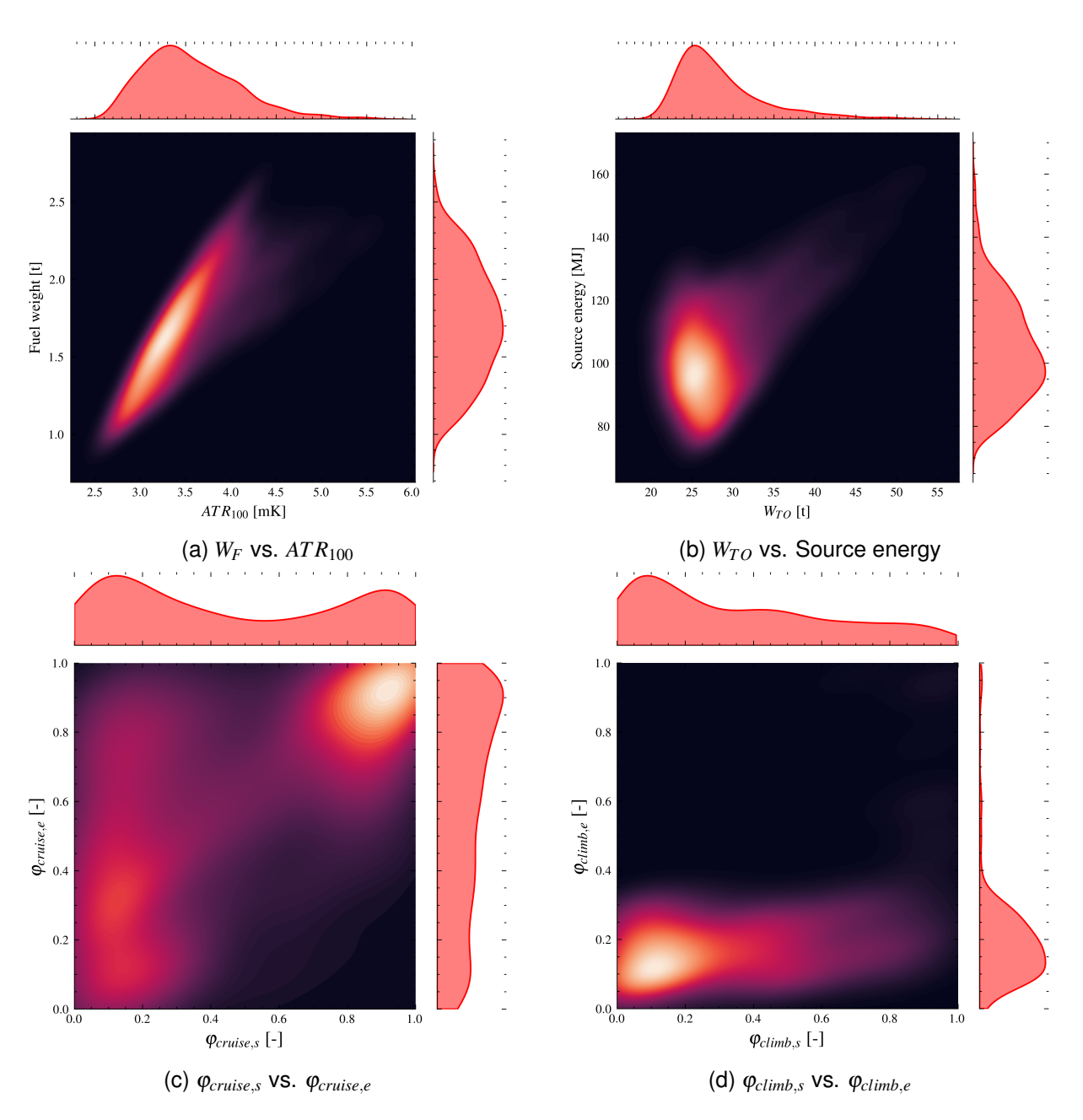


Figure 10 – Joint probability function with marginal distributions of optimized design for the Jet A1 + EU 2021 case.

Fig. 11. A similar disposition of DVs is observed, proving that the WTT scenario does not impact the choice of in-flight power management. However, the ATR_{100} and the source energy show significantly higher values due to the costly e-fuel production process. Hence, a constraint on ATR_{100} to values comparable to the baseline case is introduced in Fig. 11. The feasible designs, colored in green, only arise from values of e_{bat} greater than 1.2 kWh/kg, demonstrating the existence of a SAF paradox [63]: sustainable fuels offer themselves to be the near-term solution to aviation decarbonization, although their climate impact reduction effects become relevant when the electric mix is predominantly composed by renewable sources or hybrid powertrain solutions with high-performance battery are adopted.

Lastly, a direct comparison of observable distributions between the traditional aircraft and the e-fuel produced with the 2050 electric mix is presented in Fig. 12. The objective functions are plotted against the integral energy split Ψ . One key observation concerns the different maximum Ψ values for the two WTT scenarios: as E_{fuel} increases due to the energy consumed during e-fuel synthesis, the numerator of Eq. 5 rises. The top panels of Fig. 12 show that the energy carrier sources do not influence the distribution of fuel and take-off weights, resulting in the optimizer returning the same Pareto solutions. When the newly introduced objectives are analyzed, two distinct solution families emerge. The climate impact of the e-fuel is halved compared to the traditional configuration. Considering the design point related to the e-fuel case and highlighted in Fig. 12, obtained with the most efficient battery when $E_{electric}$ accounts for approximately 20% of the total energy supply, its ATR_{100} crosses the 1.0mK threshold. Nevertheless, this temperature reduction comes with a significant increase in the energy expended per flight, but still of the same order of magnitude as the reference value of Tab. 7. The selected design point data is reported in Tab. 9 and compared to the calculated design on ATR 42 configuration. Despite a 45.3% increase in W_{TO} , the block fuel for the 400 NM mission is significantly reduced due to the oversized battery pack.

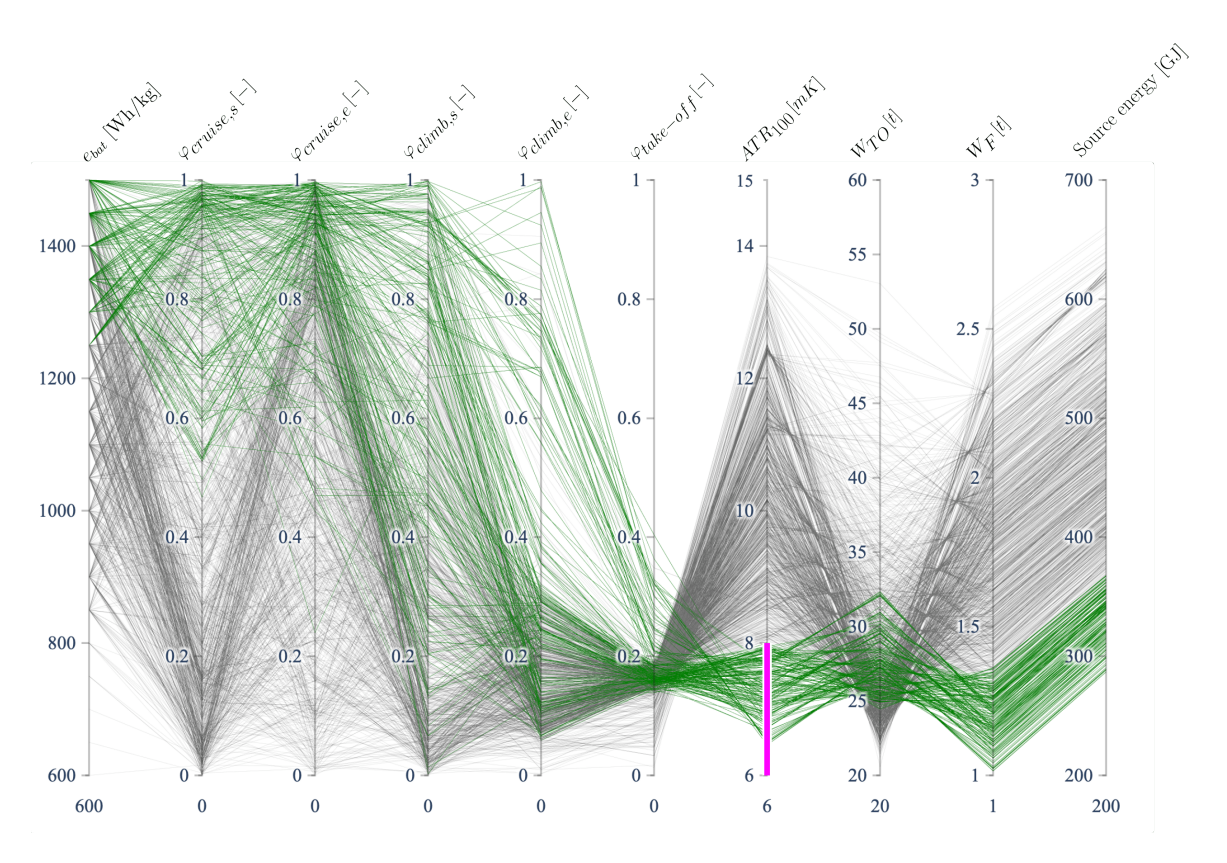


Figure 11 – Pareto-optimal solutions visualized on parallel coordinates (e_bat , 5 design variables and 4 objectives) for the FT e-fuel (EU 2021, SMR, CC) case. Green lines indicate the feasible designs according to the constraint on ATR_{100} (pink line).

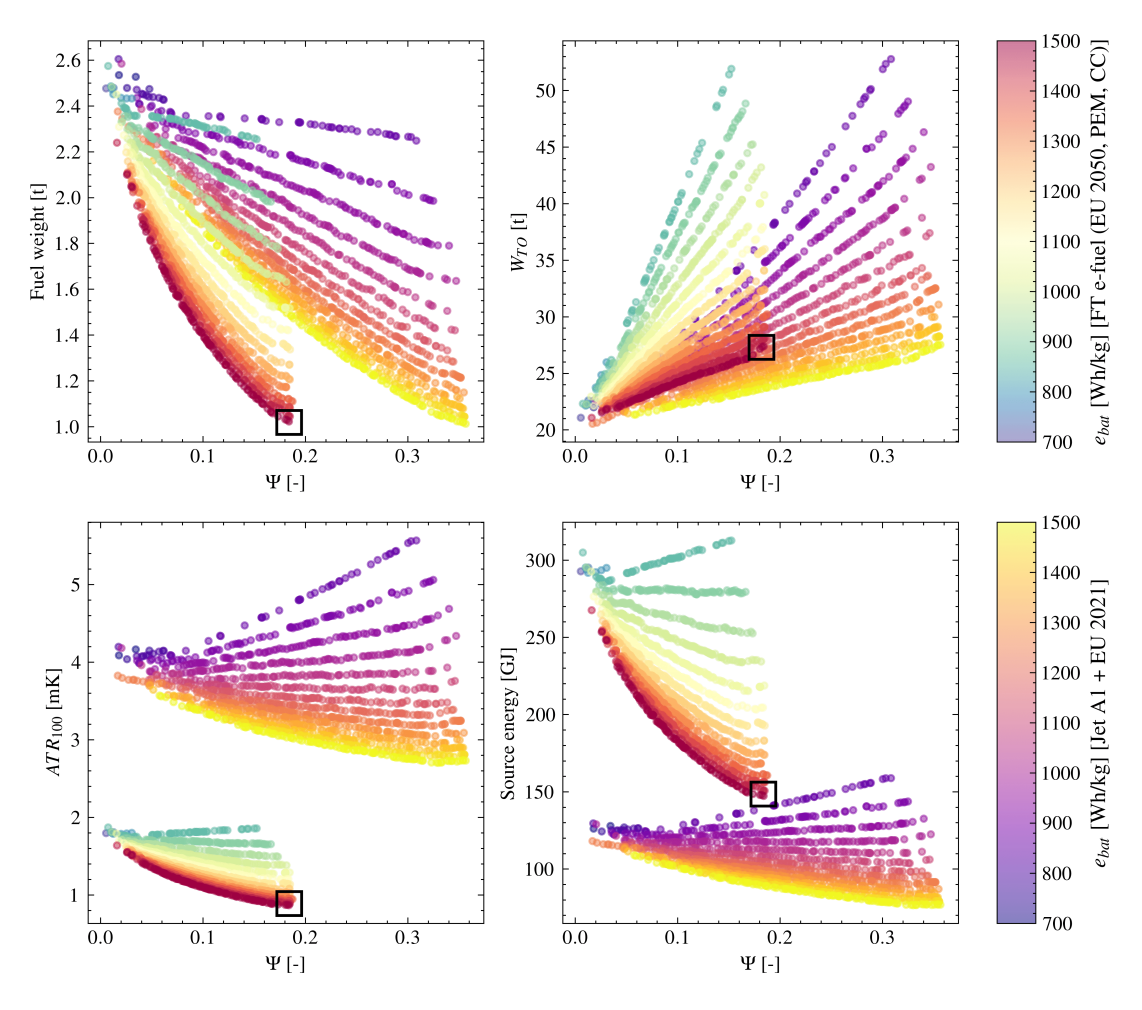


Figure 12 – Objective functions plotted against the energy split Ψ for the Jet A1 + EU 2021 and FT e-fuel (EU 2050, PEM, CC) scenarios.

Parameter	Baseline	Optimized	Difference
Take-off weight, W_{TO} [kg]	18846.43	27387.77	+45.3%
Operational Empty Weight, OEI [kg]	11811.31	16504.49	+39.7%
Powertrain weight, W_{PT} [kg]	1016.02	1375.10	+35.3%
Wing surface, $S[m^2]$	55.54	80.71	+45.3%
Block fuel (400 NM range), $W_{F,400}$ [kg]	1059.23	166.91	-84.2%
Block fuel (design range), W_F [kg]	2583.60	1022.80	-60.4%
Average temperature response, ATR_{100} [mK]	3.87	0.87	-77.5%
Source energy [GJ]	119.92	147.34	+22.9%

Table 9 – Data related to the highlighted design in Fig. 12. The percentual differences are computed using the outcome of PhlyGreen on the baseline configuration.

6. Conclusions

To address the impact of disrupting technologies in the aviation sector, such as the employment of hybrid powertrains supplied by alternative jet fuels and battery sources, extensive parametric and optimization analyses have been carried out over five different combinations of energy carriers. A set of efficiencies and emissions data have been generated through the GREET module for the lifecycle assessment of alternative fuels. When an e-fuel is produced using Fischer-Tropsch synthesis, the electricity grid mix plays a major role since the sign of the emitted CO_2 changes when moving from today's sources to the 2050 projection for the European mix. In fact, if carbon capture technologies are employed nowadays, the emitted carbon dioxide would not be balanced by the captured

CO₂ from the atmosphere. Additionally, the hydrogen production process heavily impacts the overall efficiency of the SAF generation branch. A preliminary parametric analysis performed over the baseline regional aircraft with a battery characterized by moderate/high specific energy points out the different contributions of WTT scenarios over the in-flight hybridization strategy. The adoption of a partially or fully electric powertrain marginally reduces the climate impact and the total energy required for the mission while utilizing an e-fuel produced using renewable energy drastically reduces the average temperature response of one order of magnitude with respect to the considered baseline aircraft. This analysis is extended within an optimization framework where four different objectives are minimized using the supplied power ratio related to the take-off, climb, and cruise phases as design variables. The results obtained for the kerosene-fueled aircraft reveal the preferred hybridization strategies by the optimizer, which tend to reduce the electric power supply during the peaks of required propulsive power, i.e., during the take-off and between the top of climb and the initial phases of the cruise, to avoid a battery pack oversizing. When the results for the FT e-fuel coupled with the 2021 grid mix are analyzed, a downgrade of the ATR_{100} and source energy objectives is observed: acceptable designs in terms of climate effect can be obtained with high battery specific powers. This performance degeneration overshadows the possibility of using SAFs as a near-term solution for aviation decarbonization. On the other hand, selecting a WTT scenario wherein the electric mixed is composed of a larger share of renewable energy, the overall climate impact of the entire life cycle can be reduced in response to a more energy-demanding WTT chain.

In conclusion, the present analysis brings out the different impacts of Well-to-Tank routes and hybridization strategies on the energetic and climatic targets, highlighting how the former feature is the most critical for achieving the milestones imposed by institutions and governments. The electrification of aero-engines leads to further improvements in climate figures, especially in reducing the energy consumption of SAF synthesis processes. The combination of optimized on-board power management and negative-emission e-fuel pathway can foster a carbon-neutral future for aviation.

Copyright Statement

The authors confirm that they, and/or their company or organization, hold copyright on all of the original material included in this paper. The authors also confirm that they have obtained permission, from the copyright holder of any third party material included in this paper, to publish it as part of their paper. The authors confirm that they give permission, or have obtained permission from the copyright holder of this paper, for the publication and distribution of this paper as part of the ICAS proceedings or as individual off-prints from the proceedings.

Acknowledgments

This work is part of the research activity developed by the authors within the framework of the "PNRR" CN4 MOST (Mobilità sostenibile): SPOKE 1 (Air Mobility), WP5: "Multidisciplinary design optimization and innovative solutions for next generation green aircraft with demonstrator". RMG acknowledges the financial support from the Italian Ministry of University and Research in the framework of the project "National Center for "HPC, Big Data and QC" funded by EU – NextGenerationEU. The authors acknowledge the contributions of Valeria Falcone and Chiara Nallo for their dedicated efforts and insightful contributions during their master's theses, which significantly enriched this research endeavor.

References

- [1] IATA. https://www.iata.org/en/pressroom/2022-releases/2022-03-01-01, 2022. Accessed: 2024-05-11.
- [2] D.S. Lee, D.W. Fahey, A. Skowron, M.R. Allen, U. Burkhardt, Q. Chen, S.J. Doherty, S. Freeman, P.M. Forster, J. Fuglestvedt, A. Gettelman, R.R. De León, L.L. Lim, M.T. Lund, R.J. Millar, B. Owen, J.E. Penner, G. Pitari, M.J. Prather, R. Sausen, and L.J. Wilcox. The contribution of global aviation to anthropogenic climate forcing for 2000 to 2018. *Atmospheric Environment*, 244:117834, 2021.
- [3] European Commission. A European Green Deal. https://commission.europa.eu/strategy-and-policy/priorities-2019-2024/european-green-deal_en, 2023. Accessed: 2023-11-21.

- [4] Jason Welstead and James L Felder. Conceptual design of a single-aisle turboelectric commercial transport with fuselage boundary layer ingestion. In *54th AIAA aerospace sciences meeting*, page 1027, 2016.
- [5] Askin T Isikveren, Sascha Kaiser, Clément Pornet, and Patrick C Vratny. Pre-design strategies and sizing techniques for dual-energy aircraft. *Aircraft Engineering and Aerospace Technology: An International Journal*, 86(6):525–542, 2014.
- [6] Kevin R Antcliff, Mark D Guynn, Ty Marien, Douglas P Wells, Steven J Schneider, and Michael J Tong. Mission analysis and aircraft sizing of a hybrid-electric regional aircraft. In *54th AIAA aerospace sciences meeting*, page 1028, 2016.
- [7] Robert Cameron Bolam, Yuriy Vagapov, and Alecksey Anuchin. Review of electrically powered propulsion for aircraft. In *2018 53rd international universities power engineering conference (UPEC)*, pages 1–6. IEEE, 2018.
- [8] Grigorii Soloveichik. Electrified future of aviation: batteries or fuel cells? *The Advanced Research Projects Agency—Energy (ARPA-E): Washington, DC, USA*, 2019.
- [9] Ivo Abrantes, Ana F. Ferreira, André Silva, and Mário Costa. Sustainable aviation fuels and imminent technologies CO2 emissions evolution towards 2050. *Journal of Cleaner Production*, 313, 9 2021.
- [10] A Contreras, S Yiğit, K Özay, and TN Veziroğlu. Hydrogen as aviation fuel: a comparison with hydrocarbon fuels. *International Journal of Hydrogen Energy*, 22(10-11):1053–1060, 1997.
- [11] Daniel A Crowl and Young-Do Jo. The hazards and risks of hydrogen. *Journal of Loss Prevention in the Process Industries*, 20(2):158–164, 2007.
- [12] Bhupendra Khandelwal, Adam Karakurt, Paulas R Sekaran, Vishal Sethi, and Riti Singh. Hydrogen powered aircraft: The future of air transport. *Progress in Aerospace Sciences*, 60:45–59, 2013.
- [13] European Commission. European Green Deal: new law agreed to cut aviation emissions by promoting sustainable aviation fuels. https://ec.europa.eu/commission/presscorner/detail/en/ip_23_2389, 2023. Accessed: 2023-05-15.
- [14] Vamsikrishna Undavalli, Olanrewaju Bilikis Gbadamosi Olatunde, Rahim Boylu, Chuming Wei, Josh Haeker, Jerry Hamilton, and Bhupendra Khandelwal. Recent advancements in sustainable aviation fuels. *Progress in Aerospace Sciences*, 136, 1 2023.
- [15] Meredith Colket, Joshua Heyne, Mark Rumizen, Mohan Gupta, Tim Edwards, William M. Roquemore, Gurhan Andac, Randy Boehm, Jeffery Lovett, Randy Williams, Jamey Condevaux, David Turner, Nader Rizk, Julian Tishkoff, Chiping Li, Jeff Moder, Daniel Friend, and Vaidya Sankaran. Overview of the National Jet Fuels Combustion Program. *AIAA Journal*, 55(4):1087–1104, 2017.
- [16] A4E, CANSO, ERA, ACI, ASD. Destination 2050 A route to net zero European aviation. https://www.destination2050.eu/wp-content/uploads/2021/03/Destination2050_Report.pdf, 2021. Accessed: 2023-11-30.
- [17] Ye Xie, Al Savvarisal, Antonios Tsourdos, Dan Zhang, and Jason Gu. Review of hybrid electric powered aircraft, its conceptual design and energy management methodologies. *Chinese Journal of Aeronautics*, 34:432–450, 4 2021.
- [18] Jan Roskam. Airplane design. DARcorporation, 1985.
- [19] Egbert Torenbeek. Synthesis of subsonic airplane design: an introduction to the preliminary design of subsonic general aviation and transport aircraft, with emphasis on layout, aerodynamic design, propulsion and performance. Springer Science & Business Media, 2013.
- [20] Clément Pornet, Corin Gologan, Patrick C Vratny, Arne Seitz, Oliver Schmitz, Askin T Isikveren, and Mirko Hornung. Methodology for sizing and performance assessment of hybrid energy aircraft. *Journal* of Aircraft, 52(1):341–352, 2015.
- [21] Jacopo Zamboni, Roelof Vos, Mathias Emeneth, and Alexander Schneegans. A method for the conceptual design of hybrid electric aircraft. In *AIAA scitech 2019 forum*, page 1587, 2019.
- [22] Christopher Hall, Chrysoula L Pastra, Andrew Burrell, Jonathan Gladin, and Dimitri N Mavris. Projecting power converter specific power through 2050 for aerospace applications. In *2022 IEEE Transportation Electrification Conference & Expo (ITEC)*, pages 760–765. IEEE, 2022.
- [23] Jaylon Uzodinma, Turab Zaidi, Miguel Walter, Raphael Gautier, and Dimitri N Mavris. Uncertainty Quantification on a Parallel Hybrid-Electric Propulsion EPFD Vehicle. In AIAA SCITECH 2023 Forum, page 0839, 2023.
- [24] Raphael H Gautier, Lloyd Teta, Jaylon Uzodinma, Tavish Pattanayak, Miguel Walter, Turab Zaidi, and Dimitri N Mavris. Impact of Technological Uncertainty on Design Parameter Selection of the NASA Parallel Hybrid-Electric Propulsion EPFD Vehicle. In *AIAA AVIATION 2023 Forum*, page 4501, 2023.
- [25] Higor L Silva, Gustavo J Resende, Roberto MC Neto, André RD Carvalho, Alexandre A Gil, Mateus AA

- Cruz, and Thiago AM Guimarães. A multidisciplinary design optimization for conceptual design of hybridelectric aircraft. *Structural and Multidisciplinary Optimization*, 64(6):3505–3526, 2021.
- [26] Francesco Orefice, Pierluigi Della Vecchia, Danilo Ciliberti, and Fabrizio Nicolosi. Aircraft conceptual design including powertrain system architecture and distributed propulsion. In 2019 AIAA/IEEE Electric Aircraft Technologies Symposium (EATS), pages 1–20. IEEE, 2019.
- [27] Katja Oehmichen, Stefan Majer, Franziska Müller-Langer, and Daniela Thrän. Comprehensive LCA of Biobased Sustainable Aviation Fuels and JET A-1 Multiblend. *Applied Sciences*, 12(7):3372, 2022.
- [28] Xuancan Zhu, Wenwen Xie, Junye Wu, Yihe Miao, Chengjie Xiang, Chunping Chen, Bingyao Ge, Zhuozhen Gan, Fan Yang, Man Zhang, et al. Recent advances in direct air capture by adsorption. *Chemical Society Reviews*, 2022.
- [29] Reynard de Vries, Malcom T Brown, and Roelof Vos. A preliminary sizing method for hybrid-electric aircraft including aero-propulsive interaction effects. In *2018 Aviation Technology, Integration, and Operations Conference*, page 4228, 2018.
- [30] Reynard De Vries, Malcom Brown, and Roelof Vos. Preliminary sizing method for hybrid-electric distributed-propulsion aircraft. *Journal of Aircraft*, 56(6):2172–2188, 2019.
- [31] Jack D Mattingly. Aircraft engine design. AIAA, 2002.
- [32] Guiyan Zang, Pingping Sun, Eunji Yoo, Amgad Elgowainy, Adarsh Bafana, Uisung Lee, Michael Wang, and Sarang Supekar. Synthetic Methanol/Fischer–Tropsch Fuel Production Capacity, Cost, and Carbon Intensity Utilizing CO_2 from Industrial and Power Plants in the United States. *Environmental Science & Technology*, 55(11):7595–7604, 2021. PMID: 33979128.
- [33] lea. World Energy Statistics and balances data product. https://www.iea.org/data-and-statistics/data-product/world-energy-statistics-and-balances. Accessed: 2024-05-02.
- [34] lea. Net zero by 2050 analysis. https://www.iea.org/reports/net-zero-by-2050. Accessed: 2024-05-02.
- [35] Argonne National Laboratory. GREET model. https://greet.anl.gov/databases, 2023. Accessed: 2023-11-22.
- [36] Commission Regulation (EU). Directive (EU) 2018/2001 of the European Parliament and of the Council. https://eur-lex.europa.eu/legal-content/EN/TXT/?uri=CELEX%3A32022R0720, 2020. Accessed: 2023-11-22.
- [37] Environmental Protection Agency. Renewable Fuel Standard (RFS) Program: Standards for 2023–2025 and Other Changes. https://www.govinfo.gov/content/pkg/FR-2023-07-12/pdf/2023-13462.pdf, 2023. Accessed: 2023-11-22.
- [38] Matteo Prussi, Uisung Lee, Michael Wang, Robert Malina, Hugo Valin, Farzad Taheripour, César Velarde, Mark D Staples, Laura Lonza, and James I Hileman. CORSIA: The first internationally adopted approach to calculate life-cycle GHG emissions for aviation fuels. *Renewable and Sustainable Energy Reviews*, 150:111398, 2021.
- [39] V. Grewe and K. Dahlmann. How ambiguous are climate metrics? and are we prepared to assess and compare the climate impact of new air traffic technologies? *Atmospheric Environment*, 104, 2015.
- [40] L. Megill, K. Deck, and V. Grewe. Alternative climate metrics to the Global Warming Potential are more suitabile for assessing aviation non- CO_2 effects. *Communications Earth & Environment*, 5, 2024.
- [41] Ulrich Schumann. Über Bedingungen zur Bildung von Kondensstreifen aus Flugzeugabgasen. *Meteorologische Zeitschrift*, 5(1):4–23, 1996.
- [42] Pieter-Jan Proesmans and Roelof Vos. Airplane design optimization for minimal global warming impact. *Journal of Aircraft*, 59(5):1363–1381, 2022.
- [43] Milind Kandlikar. Indices for comparing greenhouse gas emissions: integrating science and economics. *Energy Economics*, 18(4):265–281, 1996.
- [44] Emily Schwartz Dallara, Ilan M Kroo, and Ian A Waitz. Metric for comparing lifetime average climate impact of aircraft. *AIAA journal*, 49(8):1600–1613, 2011.
- [45] Robert Sausen and Ulrich Schumann. Estimates of the climate response to aircraft CO_2 and NO_x emissions scenarios. *Climatic Change*, 44:27–58, 2000.
- [46] Keith P Shine, Jan S Fuglestvedt, Kinfe Hailemariam, and Nicola Stuber. Alternatives to the global warming potential for comparing climate impacts of emissions of greenhouse gases. *Climatic change*, 68(3):281–302, 2005.
- [47] K. Hasselmann, R. Sausen, E. Maier-Reimer, and R. Voss. On the Cold Start Problem in Transient Simulations with Coupled Atmosphere-Ocean Models. *Climate Dynamics*, 9:53–61, 1993.
- [48] K. Hasselmann, S. Hasselmann, R. Giering, V. Ocana, and H. von Storch. Sensitivity Study of Opti-

- mal CO2 Emission Paths Using a Simplified Structural Integrated Assessment Model (SIAM). *Climatic Change*, 37:345–386, 1997.
- [49] IPCC. Contributions to the Fourth Assessment Report of the Intergovernmental Panel of Climate Change. Cambridge University Press, New York, NY, USA, 2007.
- [50] Volker Grewe and Andrea Stenke. AirClim: an efficient tool for climate evaluation of aircraft technology. *Atmospheric Chemistry and Physics*, 8(16):4621–4639, 2008.
- [51] Antonio Filippone and Nicholas Bojdo. Statistical model for gas turbine engines exhaust emissions. *Transportation Research Part D: Transport and Environment*, 59:451–463, 2018.
- [52] Joyce E Penner, David H Lister, David J Griggs, David J Dokken, and Mack McFarland. Intergovernmental Panel on Climate Change (IPCC). *Aviation and the Global Atmosphere Special Report, Cambridge University Press, UK*, page 373, 1999.
- [53] Planespotters.net. [atr 42 production list]. https://www.planespotters.net/aircraft/production/atr-42?sort=status, 2024. Accessed: 2024-05-02.
- [54] R Thijssen, P Proesmans, and Roelof Vos. Propeller Aircraft Design Optimization for Climate Impact Reduction. In *33rd Congress of the International Council of the Aeronautical Sciences, ICAS 2022*, page ICAS2022_0819. International Council of the Aeronautical Science (ICAS), 2022.
- [55] Andrea Spinelli, Hossein Balaghi Enalou, Bahareh Zaghari, Timoleon Kipouros, and Panagiotis Laskaridis. Application of probabilistic set-based design exploration on the energy management of a hybrid-electric aircraft. *Aerospace*, 9(3):147, 2022.
- [56] Julian Blank and Kalyanmoy Deb. Pymoo: Multi-objective optimization in python. *leee access*, 8:89497–89509, 2020.
- [57] Fancesco Orefice, Salvatore Corcione, Fabrizio Nicolosi, Danilo Ciliberti, and Giuseppe De Rosa. Performance calculation for hybrid-electric aircraft integrating aero-propulsive interactions. In AIAA Scitech 2021 Forum, page 1640, 2021.
- [58] ATR 42 datasheet. https://www.atr-aircraft.com/aircraft-services/aircraft-family/atr-42-600/, 2024. Accessed: 2024-05-11.
- [59] Kathleen A Mar, Charlotte Unger, Ludmila Walderdorff, and Tim Butler. Beyond CO_2 equivalence: The impacts of methane on climate, ecosystems, and health. *Environmental science & policy*, 134:127–136, 2022.
- [60] Modalities, procedures and guidelines for the transparency framework for action and support referred to in article 13 of the paris agreement. https://unfccc.int/resource/tet/0/00mpg.pdf. Accessed: 2024-05-02.
- [61] Alexander I Ikeuba, Prince C Iwuji, Ini-Ibehe E Nabuk, Okama E Obono, Destiny Charlie, Arit A Etim, Ben I Nwabueze, and Joseph Amajama. Advances on lithium, magnesium, zinc, and iron-air batteries as energy delivery devices—a critical review. *Journal of Solid State Electrochemistry*, pages 1–27, 2024.
- [62] Annex 14 to the Convention on International Civil Aviation. https://www.icao.int/APAC/Meetings/2015%20WAWG1/an14_led_1951.pdf. Accessed: 2024-05-30.
- [63] Reynard de Vries, Rob E Wolleswinkel, Maurice Hoogreef, and Roelof Vos. A New Perspective on Battery-Electric Aviation, Part II: Conceptual Design of a 90-Seater. In AIAA SCITECH 2024 Forum, page 1490, 2024.